

Practical Multispectral Lighting Reproduction

Chloe LeGendre* Xueming Yu Dai Liu Jay Busch
USC Institute for Creative Technologies

Andrew Jones Sumanta Pattanaik† Paul Debevec
†University of Central Florida

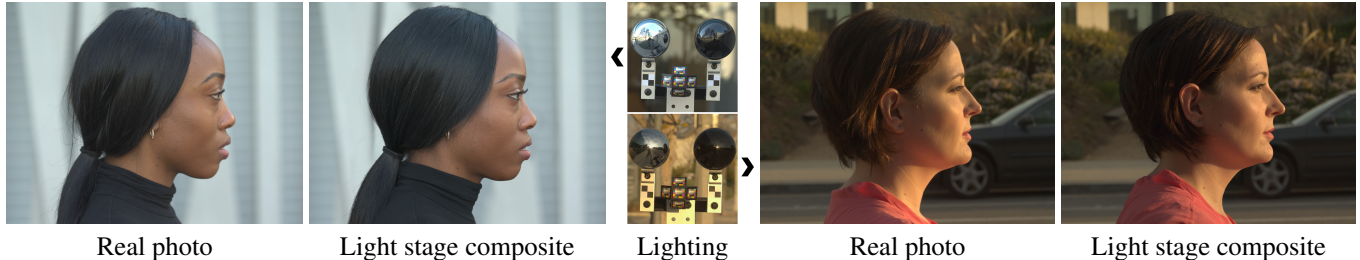


Figure 1: The left images show subjects photographed in real outdoor lighting environments. The lighting was captured with panoramic HDR images and color charts, allowing six-channel multispectral lighting reproduction. The right images show the subjects photographed inside the multispectral light stage under reproductions of the captured lighting environments, composited into background photos, producing close matches to the originals.

Abstract

We present a practical framework for reproducing omnidirectional incident illumination conditions with complex spectra using a light stage with multispectral LED lights. For lighting acquisition, we augment standard RGB panoramic photography with one or more observations of a color chart with numerous reflectance spectra. We then solve for how to drive the multispectral light sources so that they best reproduce the appearance of the color charts in the original lighting. Even when solving for non-negative intensities, we show that accurate lighting reproduction is achievable using just four or six distinct LED spectra for a wide range of incident illumination spectra. A significant benefit of our approach is that it does not require the use of specialized equipment (other than the light stage) such as monochromators, spectroradiometers, or explicit knowledge of the LED power spectra, camera spectral response functions, or color chart reflectance spectra. We describe two simple devices for multispectral lighting capture, one for slow measurements of detailed angular spectral detail, and one for fast measurements with coarse angular detail. We validate the approach by realistically compositing real subjects into acquired lighting environments, showing accurate matches to how the subject would actually look within the environments, even for those including complex multispectral illumination. We also demonstrate dynamic lighting capture and playback using the technique.

Keywords: Multispectral, Relighting, Image-Based Lighting

Concepts: •Computing methodologies → Image manipulation; Computational photography;

* e-mail:legendre@ict.usc.edu

Permission to make digital or hard copies of all or part of this work for personal or classroom use is granted without fee provided that copies are not made or distributed for profit or commercial advantage and that copies bear this notice and the full citation on the first page. Copyrights for components of this work owned by others than the author(s) must be honored. Abstracting with credit is permitted. To copy otherwise, or republish, to post on servers or to redistribute to lists, requires prior specific permission and/or a fee. Request permissions from permissions@acm.org. © 2016 Copyright held by the owner/author(s). Publication rights licensed to ACM.

SIGGRAPH '16 Technical Paper, July 24 - 28, 2016, Anaheim, CA,
ISBN: 978-1-4503-4279-7/16/07...\$15.00
DOI: <http://dx.doi.org/10.1145/2897824.2925934>

ACM Reference Format
LeGendre, C., Yu, X., Liu, D., Busch, J., Jones, A., Pattanaik, S., Debevec, P. 2016. Practical Multispectral Lighting Reproduction. ACM Trans. Graph. 35, 4, Article 32 (July 2016), 11 pages.
DOI = 10.1145/2897824.2925934 <http://doi.acm.org/10.1145/2897824.2925934>.

1 Introduction

Lighting greatly influences how a subject appears in both a photometric and aesthetic sense. And when a subject recorded in a studio is composited into a real or virtual environment, their lighting will either complement or detract from the illusion that they are actually present within the scene. Thus, being able to match studio lighting to real-world illumination environments is a useful capability for visual effects, studio photography, and in designing consumer products, garments, and cosmetics.

Lighting reproduction systems as in Debevec et al. [2002] and Harmon et al. [2014] surround a subject with red, green, and blue light-emitting diodes (RGB LEDs) and drive them to match the colors and intensities of the lighting of the scene into which the subject will be composited. The lighting environments are typically recorded as omnidirectional, high dynamic range (HDR) RGB images photographed using panoramic photography or computed in a virtual scene using a global illumination algorithm. While the results can be believable – especially under the stewardship of color correction artists – the accuracy of the color rendition is suspect since only RGB colors are used for recording and reproducing the illumination, and there is significantly more detail across the visible spectrum than what is being recorded and simulated. Wenger et al. [2003] noted that lighting reproduced with RGB LEDs can produce unexpected color casts even when each light source strives to mimic the directly observable color of the original illumination. Ideally, a lighting reproduction system could faithfully match the appearance of the subject under any combination of illuminants including incandescent, daylight, fluorescent, solid-state, and any filtered or reflected version of such illumination.

Recently, several efforts have produced multispectral light stages with more than just red, green, and blue LEDs in each light source for purposes such as multispectral material measurement [Gu and Liu 2012; Ajdin et al. 2012; Kitahara et al. 2015]. These systems add additional LED colors such as amber and cyan, as well as white LEDs that use phosphors to broaden their emission across the visible spectrum. In this work, we present a practical technique for driving the intensities of such arrangements of LEDs to accurately reproduce the effects of real-world illumination environments with any number of spectrally distinct illuminants in the scene. The practical nature of our approach rests in that we do not require explicit spectroradiometer measurements of the illumination; we use only

traditional HDR panoramic photography and one or more observations of a color chart reflecting different directions of the illumination in the environment. Furthermore, we drive the LED intensities directly from the color chart observations and HDR panoramas, without explicitly estimating illuminant spectra, and without knowledge of the reflectance spectra of the color chart samples, the emission spectra of LEDs, or the spectral sensitivity functions of the cameras involved. Our straightforward process is:

1. Photograph the color chart under each of the different LEDs
2. Record scene illumination using panoramic photography plus observations of a color chart facing one or more directions
3. For each LED light source, estimate the appearance of a virtual color chart reflecting its direction of light from the environment
4. Drive the light source LEDs so that they best illuminate the virtual color chart with the estimated appearance

Step one is simple, and step four simply uses a nonnegative least squares solver. For step two, we present two assemblies for capturing multispectral lighting environments that trade spectral angular resolution for speed of capture: one assembly acquires unique spectral signatures for each lighting direction; the other permits video rate acquisition. For step three, we present a straightforward approach to fusing RGB panoramic imagery and directional color chart observations. The result is a relatively simple and visually accurate process for driving a multispectral light stage to reproduce the spectrally complex illumination effects of real-world lighting environments. We demonstrate our approach by recording several lighting environments with natural and synthetic illumination and reproduce this illumination within an LED sphere with six distinct LED spectra. We show this enhanced lighting reproduction process produces accurate appearance matches for color charts, a still life scene, and human subjects and can be extended to real-time multispectral lighting capture and playback.

2 Background and Related Work

In this work, we are interested in capturing the incident illumination spectra arriving from all directions in a scene toward a subject, as seen by a camera. Traditional omnidirectional lighting capture techniques [Debevec 1998; Tominaga and Tanaka 2001] capture only tristimulus RGB imagery, often by photographing a mirrored sphere with a radiometrically calibrated camera. More recently, significant work has been done to estimate or capture spectral incident illumination conditions. With measured spectral camera sensitivity functions (CSF's), Tominaga and Tanaka [2006] promoted RGB spherical imagery to spectral estimates by projecting onto the first three principal components of a set of illuminant basis spectra, showing successful modeling of daylight and incandescent spectra within the same scene. However, the technique required measuring the camera CSF's and was not demonstrated to solve for more than two illuminant spectra. Kawakami et al. [2013] promoted RGB sky imagery to spectral estimates by inferring sky turbidity and fitting to a spectral skylight model. Tominaga and Fukuda [2007] acquired mirror sphere photographs with a monochrome camera and multiple bandpass filters to achieve six spectral bands and swapped the bandpass filters for a Liquid Crystal Tunable Filter to achieve 31 or 61 bands. Since the filters' bands overlapped, they solved a linear system to best estimate the illuminant spectra. However, the system required specialized equipment to achieve these results.

Capturing daylight lighting conditions has received attention of its own. Stumpfel et al. [2004] used neutral density filters and an especially broad range of high dynamic range exposures with an

upward-pointing fisheye lens to accurately record the upper hemisphere of incident illumination but did not promote RGB data to spectral measurements. Debevec et al. [2012] recorded the full dynamic range of natural illumination in a single photograph based on observed irradiance on diffuse grey strips embedded within a cut-apart mirrored sphere, allowing reconstruction of saturated light source intensities. Kider et al. [2014] augmented the fisheye capture technique of Stumpfel et al. [2004] with a mechanically instrumented spectroradiometer, capturing 81 sample spectra over the upper hemisphere. They used bicubic interpolation over the hemisphere to validate a variety of spectral sky models but did not explicitly fuse the spectral data with the RGB photography of the sky. HDR image and lighting capture has also been extended to real-time video [Kang et al. 2003; Unger and Gustavson 2007] using interleaved exposures, but only for RGB imagery.

Significant work has been done to estimate illuminant spectra and/or CSF's using color charts with samples of known or measured reflectance. The Macbeth ColorCheckerTM Chart [McCamy et al. 1976] (now sold by X-RiteTM) simulates a variety of natural reflectance spectra, including light and dark human skin, foliage, blue sky, certain types of flowers, and a ramp of spectrally flat neutral tones. Its 24 patches have 19 independent reflectance spectra, which, when photographed by an RGB camera, yield 57 linearly independent integrals of the spectrum of light falling on the chart. Rump et al. [2011] showed that CSF's could be estimated from an image of such a chart (actually, a more advanced version with added spectra) under a known illuminant, and Shi et al. [2014] showed that relatively smooth illuminant spectra could be estimated from a photograph of such a chart. Our goal is not to explicitly estimate scene illuminant spectra as in Shi et al., but rather to drive a sphere of multispectral LEDs to produce the same appearance of a subject to a camera under spectrally complex lighting environments. While neither of these works addresses omnidirectional lighting capture or lighting reproduction, both show that surprisingly rich spectral information is available from color chart observations, which we leverage in our work.

Reproducing the illumination of a real-world scene inside a studio can be performed as in Debevec et al. [2002] by surrounding the actor with computer-controlled red-green-blue LED lights and driving them to replicate the color and intensity of the scene's incident illumination from each direction. This method has been applied in commercial films such as *Gravity* [Hamon et al. 2014]. Wenger et al. [2003] showed, however, that using only red, green, and blue LEDs significantly limits the color rendition quality of the system. To address this, they showed that by measuring the spectra of the LEDs, the spectral reflectance of a set of material samples, and the camera's spectral sensitivity functions, the color rendition properties of particular illuminants such as incandescent and fluorescent lights could be simulated reasonably well with a nine-channel multispectral LED light source. However, this work required specialized measurement equipment and limited discussion to individual light sources, not fully spherical lighting environments. Park et al. [2007] estimated material reflectance spectra using time-multiplexed multispectral lighting, producing video-rate multispectral measurements and achieving superior relighting results as compared with applying a color matrix. However, the approach also required measurement of camera spectral sensitivities and LED emission spectra and did not consider complex spherical illumination environments for relighting. Since then, a variety of LED sphere systems have been built with greater spectral resolution, including the 6-spectrum system of Gu and Liu [2012], the 16-spectrum system of Ajdin et al. [2012], and the 9-spectrum system of Kitahara et al. [2015]. In our work, we use a six-channel multispectral light stage, but instead of using multiple lighting conditions to perform reflectance measurement, we drive the multi-

spectral LEDs in a single lighting condition that optimally reproduces the appearance the subject would have in the environment. And importantly, we perform this with an easy-to-practice system for recording the spectral properties of the illumination and driving the LED light sources accordingly, without the need for specialized equipment beyond the light stage itself.

3 Method

In this section we describe our techniques for capturing incident illumination and driving multispectral light sources in order to reproduce the effect of the illumination on a subject as seen by a camera.

3.1 Driving Multispectral Lights with a Color Chart

We first consider the sub-problem of reproducing the appearance of a color chart to a given camera in a particular lighting environment using a multispectral light source. Photographing the chart with an RGB camera produces pixel values P_{ij} where i is the index of the given color chart patch and j is the camera's j 'th color channel. Because light is linear, the superposition principle states that the chart's appearance to the camera under the multispectral light source will be a linear combination of its appearance under each of the spectrally distinct LEDs. Thus, we record the basis for every way the chart can appear by photographing the chart lit by each of the LED spectra at unit intensity to produce images as seen in Fig. 3. We then construct a matrix \mathbf{L} where L_{ijk} is the averaged pixel value of color chart square i for camera color channel j under LED spectrum k . To achieve even lighting, we do this using the full sphere of LED sphere light sources of a given spectrum simultaneously, though a single multispectral light could be used. We consider \mathbf{L} to be the $ij \times k$ matrix whose columns correspond to the LED spectrum k and whose rows unroll the indices i and j to place the RGB pixel values for all chart squares in the same column. To optimally reproduce the chart appearance, we simply need to solve for the LED intensity coefficients α_k that minimize Eq. 1, where m is the number of color chart patches and n is the number of different LED spectra.

$$\sum_{i=1}^m \sum_{j=1}^3 (P_{ij} - \sum_{k=1}^n \alpha_k L_{ijk})^2 = \|\mathbf{P} - \mathbf{L}\boldsymbol{\alpha}\|^2 \quad (1)$$

Conveniently, this process does not require measuring the illuminant spectra, the camera spectral sensitivity functions, the color chart's reflectance spectra, or even the spectra of the LEDs.

We can also state the problem in terms of the unknown scene illuminant spectrum $I(\lambda)$, the color chart spectral reflectance functions $R_i(\lambda)$, and the camera spectral sensitivity functions $C_j(\lambda)$, where:

$$P_{ij} = \int_{\lambda} I(\lambda) R_i(\lambda) C_j(\lambda) \quad (2)$$

If we define the emission spectrum of LED k as $I_k(\lambda)$ and drive each LED to a basis weight intensity of α_k , the reproduced appearance of the chart patches under the multispectral light is:

$$P_{ij} \approx \int_{\lambda} \left[\sum_{k=1}^n \alpha_k I_k(\lambda) \right] R_i(\lambda) C_j(\lambda) \quad (3)$$

Since α_k does not depend on λ , we can pull the summation out of the integral, which then simplifies to the appearance of the color chart patches under each of the basis LED spectra L_{ijk} :

$$P_{ij} \approx \sum_{k=1}^n \alpha_k \int_{\lambda} I_k(\lambda) R_i(\lambda) C_j(\lambda) = \sum_{k=1}^n \alpha_k L_{ijk} \quad (4)$$

Thus, everything we need to know about the spectra of the illuminant, color chart patches, LEDs, and camera sensitivities is measured directly by photographs of the color chart and without explicit spectral measurements. Of course, this technique does not specifically endeavor to reproduce the precise spectrum of the original illuminant, and with only six LED spectra this would not generally be possible. However, as more LED sources of distinct spectra are added, the reproduced illumination $\sum_{k=1}^n \alpha_k I_k(\lambda)$ will better approximate the original illuminant $I(\lambda)$.

We can easily solve for the LED intensities α_k that minimize Eq. 1 using linear least squares (LLS), but this may lead to negative weights for some of the LED colors, which is not physically realizable. We could, however, simulate such illumination by taking two photographs, one where the positively-weighted LEDs are turned on, and a second where the absolute values of the negatively-weighted LEDs are turned on, and subtract the pixel values of the second image from the first. If our camera can take these two images quickly, this might be an acceptable approach. But to avoid this complication (and facilitate motion picture recording) we can instead solve for the LED intensity weights using nonnegative least squares (NNLS), yielding the optimal solution where the lighting can be reproduced all at once and captured in a single photograph.

To test this technique, we used a Canon 1DX DSLR camera to photograph a Matte ColorChecker Nano from Edmund Optics, which includes 12 neutral squares and 18 color squares of distinct spectra [McCamy et al. 1976] under incandescent, fluorescent, and daylight illuminants. We then recorded the color chart's \mathbf{L} matrix under our six LED spectra (Fig. 2) producing the images in Fig. 3.

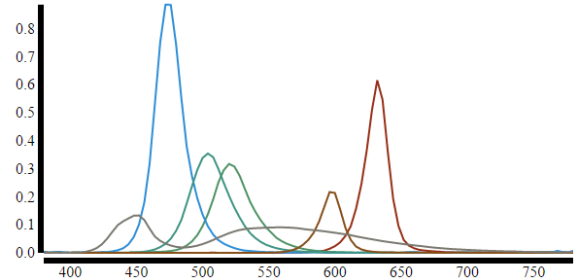


Figure 2: The illumination spectra of the six LEDs in each light source of the LED sphere.

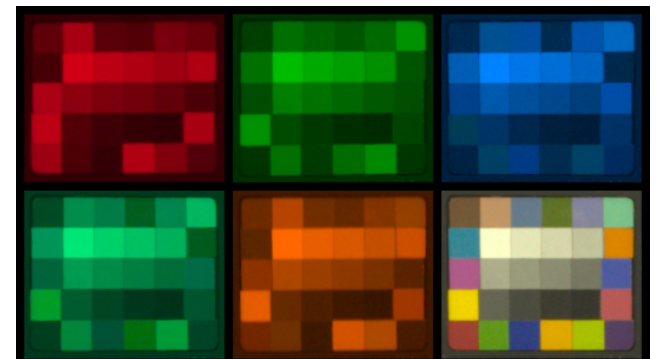


Figure 3: The color chart illuminated by the red, green, blue, cyan, amber, and white LEDs, allowing measurement of the \mathbf{L} matrix.

The background squares of the first row of Fig. 5 show the appearance¹ of the color chart under the three illuminants, while the

¹For display, RAW pixel values are converted to sRGB color space.

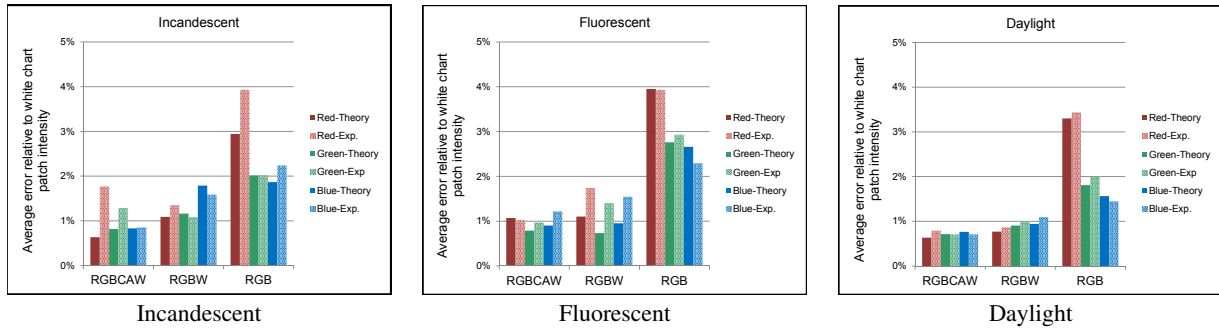


Figure 4: Quantitative error plots for Fig. 5 for different illuminants and number of LED spectra used for lighting reproduction, based on the average squared errors of raw pixel values from all 30 ColorChecker Nano patches. Both the theoretical error from the minimization and actual error from reproducing the illumination are reported.

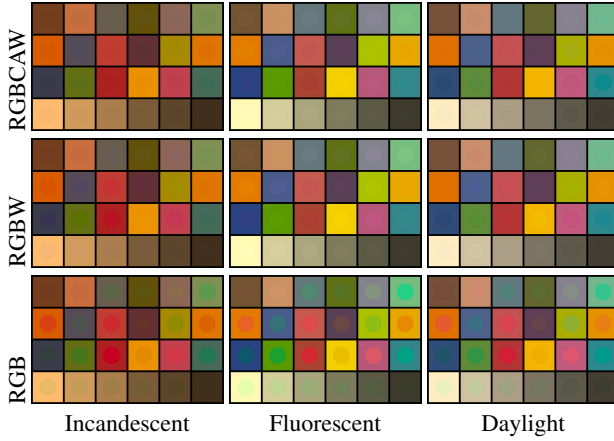


Figure 5: Comparison color charts for three illuminants where the background of each square is the original chart appearance, and the circles (sometimes invisible) show the color chart under the reproduced illumination in the LED sphere. Six (RGBCAW), four (RGBW), and three (RGB) spectral channels are used.

circles inside the squares show the appearance under the nonnegative least squares solve for six LEDs (red, green, blue, cyan, amber, and white, or RGBCAW) for direct comparison. This yields charts that are very similar in appearance, to the point that many circles are difficult to see at all. The second two rows show the results of reproducing the illumination with just four (RGBW) or three (RGB) LED spectra. The RGBW matches are also close, but the RGB matches are generally poor, producing oversaturated colors that are easily distinguishable from the original appearance. These differences are reported quantitatively in Fig. 4.

Using Different Cameras Although not preferred, cameras with differing spectral sensitivity functions may be used to record the environment lighting and the reproduced illumination, as the solving process will still endeavor to find LED intensities that reproduce the chart's appearance. Fig. 6 shows a color chart photographed under several illuminants with a Canon 1DX DSLR, and then as it appears photographed with a Nikon D90 DSLR under reproduced illumination calculated from an L matrix from the Nikon D90. Despite different sensitivities, the matches are reasonably close, with the most notable discrepancies in the blue and purple squares under fluorescent illumination. If both cameras are available to photograph a color chart in the target illumination, applying a lighting-specific 3×3 color transfer matrix first can further improve the match.

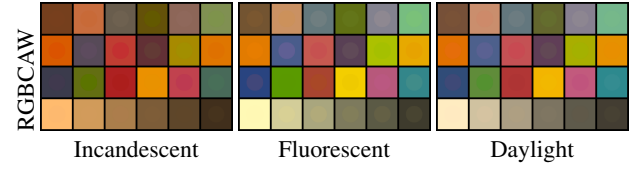


Figure 6: Charts photographed with a Canon 1DX camera (background squares) with lighting reproduced in the LED sphere photographed by a Nikon D90 camera (foreground circles).

3.2 Recording a Color Chart Panorama

Real lighting environments often feature a variety of illuminant spectra, with indirect light from numerous materials modulating these spectra. A color chart, lit by an entire hemisphere of light, lacks the angular discrimination needed to record detailed directional effects of such illumination. To address this, we built a black paper enclosure (Fig. 7) to allow only a narrow cone of light to fall on the color chart and secured it in front of a camera. We chose the cone width to roughly match the angular resolution of our light stage, which has light sources spaced 12° apart around its equator. We cover the aperture with three sheets of 5-degree light-shaping diffuser from Luminit, Inc. to antialias incident light. A printable pattern for this enclosure is provided as supplemental material.

To capture a spherical lighting environment, we place a Canon Rebel 3Ti DSLR with a Sigma 50mm macro lens with the color chart box on a GigaPan EPIC 100 pan/tilt rig, and program the rig to record the 360° environment as a set of 30 horizontal by 24 vertical directions, which roughly matches the angular resolution of the LED sphere. As the chart becomes brightly illuminated when pointed toward a light source, we set the camera to aperture-priority (Av) mode so that the shutter speed will be automatically chosen to expose the color chart properly at each position. The shutter speeds are recorded within each image's EXIF metadata. We graphed pixel values of the grayscale chart patches under fixed lighting for a range of shutter speeds, finding the "shutter speed" EXIF tag to be accurate. We cover the viewfinder to prevent stray light from reaching the light meter. Capturing the 720 images takes about one hour.

We stabilize the color chart image sequence using fiducial markers, so we may reliably sample a 20×20 pixel area in the center of each square. We divide the mean pixel values by the EXIF exposure time for each photograph, producing values proportional to the actual HDR radiance from the chart squares. By choosing an appropriate f/stop and ISO, the exposure times vary from 1/2 to 1/1000 second in a typical environment. A full lat-long panorama of charts can be seen in Fig. 8 (left). Transposing the data yields a

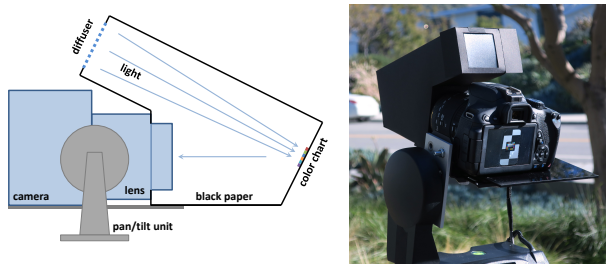


Figure 7: We use a black box to photograph a small color chart illuminated by only a small section of the environment. The box is placed over the lens of a camera on a pan/tilt rig to capture an omnidirectional multispectral lighting environment.

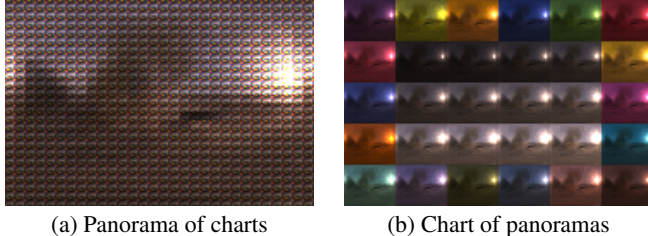


Figure 8: Two visualizations of an outdoor multispectral lighting environment recorded as a color chart panorama as in Sec. 3.2.

chart of lat-long panoramas, where each section is a low-resolution image of the environmental illumination modulated by the spectral reflectance of each chart square as in Fig. 8 (right).

3.3 Lighting a Subject with a Color Chart Panorama

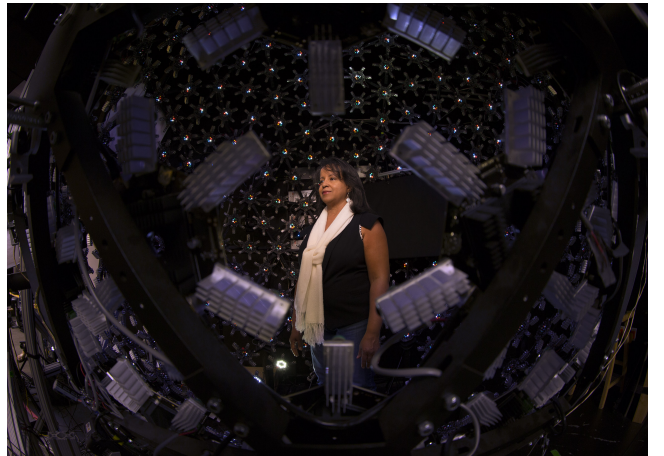
We know from Sec. 3.1 how to drive a multispectral LED source to match the appearance of a color chart, and we have now measured how each section of our lighting environment, at about the resolution of our LED sphere, illuminates a color chart. Thus, for each light source, we bilinearly interpolate the four nearest charts to the precise direction of the light to create an interpolated chart P for that light. We then drive the LEDs in the light so that it illuminates the chart as it appeared lit by the environment. The LED sphere creates varying LED intensities through pulse-width modulation (PWM), using 12 bits of lighting input to achieve 4K possible intensity values. We automatically scale the overall brightness of the lighting environment so that all of the LED intensity values fit within range, and the lighting environment is reproduced up to this scaling factor.

Fig. 9 shows a subject illuminated by two lighting environments which were spectrally recorded using the panoramic color chart technique of Sec. 3.2, next to results of driving the LED sphere with 6-channel RGBCAW LED intensities solved for from the chart data. It achieves good matches for the skin tones, clothing, and specular highlights.

3.4 Augmenting RGB Panoramas with Color Charts

Recording a lighting environment with the panoramic color chart method takes significantly longer than typical HDRI lighting capture techniques such as photographing a mirrored sphere or acquiring HDR fisheye photographs. To address this, we describe a simple process to promote a high-resolution RGB HDRI map to multispectral estimates using a sparse set of color chart observations.

Suppose that one of our LED sphere light sources is responsible for



(a) Subject in the multispectral light stage



Figure 9: (a) A fisheye view of a subject in the multispectral light stage (b) The subject in a daylight environment captured as the panorama of color charts in Fig. 8. (c) The subject in the LED sphere (a) with the lighting reproduced as in Sec. 3.3 (d) A subject in an indoor lighting environment with LED, fluorescent, and incandescent light sources also captured as a panorama of color charts. (e) The subject lit in the LED sphere with the indoor lighting.

reproducing the illumination from a particular set of pixels T in the RGB HDR panorama, and the average pixel value of this area is Q_j (where j indicates the color channel). Q 's three color channels are not enough information to drive the multispectral light source, and we wish we had seen an entire color chart lit by this part of the environment T . Suppose that we can estimate, from the sparse sampling of color charts available, the appearance of a color chart P_{ij} lit by the same general area of the environment as T , and we consider it to be reflecting an overall illuminant $I(\lambda)$ corresponding to our environment area T . Again, we presume the spectral camera model of Eq. 2, where $R_i(\lambda)$ is the spectral reflectance function of patch i of the color chart and $C_j(\lambda)$ is the spectral sensitivity function of the j 'th color channel of the camera.

$$P_{ij} = \int_{\lambda} I(\lambda) R_i(\lambda) C_j(\lambda)$$

Our color chart features a white, spectrally flat neutral square which we presume to be the zeroth index patch $R_0(\lambda) = 1$. (In practice, we scale up P_0 to account for the fact that white patch is only 90% reflective.) This patch reflects the illumination falling on the chart as seen by the camera, which yields our RGB pixel observation Q . In general, since the illuminant estimate $I(\lambda)$ corresponds to a larger area of the environment than T , Q will not be equal to P_0 . For example, if T covers an area of foliage (for example) modulating $I(\lambda)$ by spectral reflectance $S(\lambda)$, and the illuminant I broadly accounts for the incident daylight, we would have:

$$Q_j = \int_{\lambda} I(\lambda) S(\lambda) C_j(\lambda)$$

Since we want to estimate the appearance of a color chart P'_{ij} illuminated by the environment area T , we are interested in knowing

how the modulated illuminant $I(\lambda)S(\lambda)$ would illuminate the color chart squares $R_i(\lambda)$ as:

$$P'_{ij} = \int_{\lambda} I(\lambda)S(\lambda)R_i(\lambda)C_j(\lambda)$$

We do not know the spectral reflectance $S(\lambda)$, but we know that environmental reflectance functions are generally smooth, whereas illuminants can be spiky. If we assume that $S(\lambda) \approx \bar{s}_j$ over each camera sensitivity function $C_j(\lambda)$, we have:

$$P'_{ij} = \bar{s}_j \int_{\lambda} I(\lambda)R_i(\lambda)C_j(\lambda)$$

We can now write $P'_{ij} = \bar{s}_j P_{ij}$ and since $R_0(\lambda) = 1$, we can write:

$$P'_{0j} = \bar{s}_j \int_{\lambda} I(\lambda)C_j(\lambda) = Q_j$$

so $\bar{s}_j = Q_j/P_{0j}$ and we compute $P'_{ij} = Q_j P_{ij}/P_{0j}$. In effect, we divide the estimated illuminant color chart P by its white square and recolor the whole chart lit by the observed RGB pixel average Q to arrive at the estimate P' for a color chart illuminated by T . This chart is consistent with Q and retains the same relative intensities within each color channel of the estimated illuminant falling on the chart patches.

If our camera spectral response functions were known, then it might be possible to estimate $S(\lambda)$ as more than a constant per color channel to yield a more plausible P' . This is of interest to investigate in future work.

3.5 Fast Multispectral Lighting Environment Capture

Recording even a sparse set of color chart observations using the pan/tilt technique is still relatively slow compared to shooting an RGB HDR panorama. If the scene is expected to comprise principally one illuminant, such as daylight, one could promote the entire HDRI map to multispectral color information using a photograph of a single color chart to comprise every color chart estimate P' . However, for scenes with mixed illumination sources, it would be desirable to record at least some of the angular variation of the illumination spectra.

To this end, we constructed the fast multispectral lighting capture system of Fig. 10(a), which points a DSLR camera at chrome and black 8cm spheres from Dube Juggling Equipment and five Matte Nano ColorChecker charts from Edmund Optics aimed in different directions. The chrome sphere was measured to be 57.5% reflective using the reflectance measurement technique of Reinhard et al. Ch. 9 [2005]. The black acrylic sphere, included to increase the observable dynamic range of illumination, reflects 4% of the light at normal incidence, increasing significantly toward grazing angles in accordance with Fresnel's equations for a dielectric material. The five color charts face forward and point $\pm 45^\circ$ vertically and horizontally. A rigid aluminum beam secures the DSLR camera and 100mm macro lens 135cm away from the sphere and chart arrangement. Two checker fiducial markers can be used to stabilize dynamic footage if needed.

If the lighting is static, we can record an HDR exposure series and reconstruct the RGB lighting directly from the chrome sphere as in the work of Debevec [1998]. If the lighting is dynamic and must be recorded in a single shot, we can set the exposure so that the indirect light from the walls, ceiling, or sky exposes acceptably well in the chrome ball, and that the light sources can be seen distinctly in the black ball, and combine these two reflections into an HDR map. We begin by converting each sphere reflection to a latitude-longitude (lat-long) mapping as in Reinhard et al. Ch. 9 [2005]. Since the spheres are 3° apart from each other with respect to the camera, we



Figure 10: (a) Photographer using the fast multispectral lighting capture system (b) Image from the lighting capture camera with spheres and color charts. (c) Color-coded visualization of interpolating the five charts over the front hemisphere of surface normals.

shift the black sphere lat-long image to rotate it into alignment with the mirrored sphere image. The spheres occlude each other from a modest set of side directions, so we take care to orient the device so that no major sources of illumination fall within these areas.

We correct both the chrome and black sphere maps to 100% reflectivity before combining their images in HDR. For the black ball, this involves dividing by the angularly-varying reflectivity resulting from Fresnel gain. We measured the angularly-varying reflectivity of the two spheres in a dark room, moving a diffuse light box to a range of angles incident upon the spheres, allowing us to fit a Fresnel curve with index of refraction 1.51 to produce the corrective map. Since the dielectric reflection of the black ball depends significantly on the light's polarization, we avoid using the black sphere image when reconstructing skylight.

In either the static or dynamic case, if there are still bright light sources (such as the sun) which saturate in all of the available exposures, we reconstruct their RGB intensities indirectly from the neutral grey squares of the five color charts using the single-shot light probe technique of Debevec et al. [2012]. Other dynamic RGB HDR lighting capture techniques could be employed, such as that of Unger and Gustavson [2007].

Once the RGB HDR lighting environment is assembled, we need to promote it to a multispectral record of the environment using the five color charts $P_1 \dots P_5$. For each LED sphere light, we estimate how a virtual color chart P' would appear lit by the light it is responsible for reproducing. Since we do not have a chart which points backwards, we postulate a backwards-facing color chart P_6 as the average of the five observed color charts. The six color charts now point toward the vertices of an irregular octahedron. To estimate P' , we determine which octahedral face the LED Sphere light aims toward, and compute P' as the barycentric interpolation of the charts at the face's vertices. Fig. 10(c) visualizes this interpolation map over the forward-facing directions of a diffuse sphere.

We are nearly ready to drive the LED sphere with the captured multispectral illumination. For each light, we determine the average RGB pixel color Q of the HDR lighting environment area corresponding to the light source. We then scale the color channels of our color chart estimate P to form P' consistent with Q as in Sec. 3.4. We then solve for the LED intensities which best reproduce the appearance of color chart P' using the technique of Sec. 3.1.

3.6 Reproducing Dynamic Multispectral Lighting

The fast multispectral capture system allows us to record dynamic lighting environments. Most digital cinema cameras, such as the RED Epic and ARRI Alexa, record a compressed version of RAW sensor data, which can be mapped back into radiometrically linear measurements according to the original camera response curves. While this feature is not usually present in consumer cameras, the Magic Lantern software add-on (<http://www.magiclantern.fm/>) allows many Canon DSLR cameras to record RAW video at high def-



Figure 11: (upper left) Unwrapped chrome and black acrylic sphere images from Fig. 10 in latitude-longitude mapping. (upper right) Sampled colors from the five color charts. (bottom) The six derived maps for driving the red, green, blue, cyan, amber, and white LEDs to reproduce the multispectral illumination.

inition resolution. We installed the add-on onto a Canon 5D Mark III video camera to record 24fps video of the multispectral lighting capture apparatus, which we could play back at 24fps on the LED sphere as a spherical frame sequence. Fig. 18 shows some results made using this process.

4 Results

In this section, we compare various lighting reproduction results to photographs of subjects in the original lighting environments. We tried to match poses and expressions from real to reproduced illumination, although sometimes the shoots were completed hours or a day apart. We placed a black foamcore board 1m behind the actor in the light stage (Fig. 9(a)) for a neutral background. We photographed the actors in RAW mode on a Canon 1DX DSLR camera, and no image-specific color correction was performed. To create printable images, all raw RGB pixel values were transformed to sRGB color space using the 3×3 color matrix [1.879, -0.879, 0.006; -0.228, 1.578, -0.331; 0.039, -0.696, 1.632], which boosts color saturation to account for the spectral overlap of the sensor filters. Finally, a single brightness scaling factor was applied equally to all three color channels of each image to account for the brightness variation between the real and reproduced illumination and the variations in shutter speed, aperture, and ISO settings.

Fig. 12 shows two subjects in indoor, sunlit, and cloudy lighting environments. The indoor environment featured an incandescent soft box light and spectrally distinct blue-gelled white LED light panels, with fluorescent office lighting in the ceiling. The lighting environment was recorded using the fast capture technique of Sec. 3.5, and the subject was photographed in the same environment. Later, in the LED sphere, the lighting was reproduced using nonnegative 6-channel RGBCAW lighting, 4-channel RGBW lighting, and 3-channel RGB lighting solves as described in Sec. 3.4. Generally, the matches are visually very close for RGBCAW and RGBW lighting reproduction, whereas colors appear too saturated using RGB lighting. The fact that the nonnegative RGBW lighting reproduction performs nearly as well as RGBCAW suggests that these four spectra may be sufficient for many lighting reproduction applications. The bottom rows include a sunset lighting condition

reproduced with RGBCAW lighting where the light of the setting sun was changing rapidly. We recorded the illumination both before and after photographing the subject, averaging the two sets of color charts and RGB panoramas to solve for the lighting to reproduce. In the bottom row, the subject appears somewhat shinier in the reproduced illumination, possibly because the real lighting environment photo was taken closer to the time of her makeup application.

Fig. 13 compares the results using the fast capture technique of Sec. 3.5 with the color chart panorama method of Sec. 3.2, with RGBCAW lighting reproduction for a still life scene. The recorded lighting environment included incandescent and fluorescent area light sources placed directly against the left and right sides of the light stage, allowing the lighting to be captured and reproduced by the LEDs without moving the still life or the camera. The still life contained materials with diverse reflectance spectra, including a variety of prism-shaped crayons and twelve fabric swatches arranged as a chart. We used a Canon Rebel 3Ti DSLR to capture both the lighting and the subject. Qualitatively, both illumination capture techniques produced appearances for the still life materials that closely matched those in the real illumination (center of Fig. 13).

Fig. 14 compares the results of a linear least squares (LLS) RGBCAW solve with positive and negative LED intensities to a non-negative least squares (NNLS) solve for the lighting environment of Fig. 13, using the fast illumination capture method of Sec. 3.5. The LLS solve reproduced the incandescent source with mostly positive LED intensities with a small amount of negative blue and green, and the fluorescent source as mostly positive with a small amount of negative cyan. Both solutions closely approximate the appearance of the still life in the original environment.

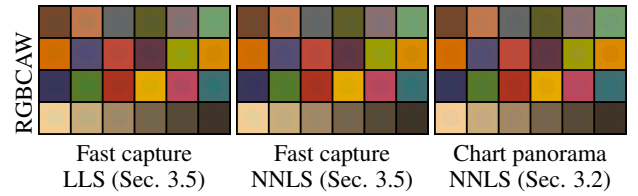


Figure 15: Charts photographed in a real lighting environment (background squares) with reproduction in the light stage (foreground circles) using LLS and NNLS 6-channel solves for the techniques of Secs. 3.5 and 3.2. Left: 3rd image of Fig. 14. Center: Last image Fig. 14. Right: 4th image of Fig. 13.

Fig. 15 shows the color chart pixel values for each of the lighting reproduction methods of Figs. 13 and 14 (foreground), compared with the values under the real illumination (background), with quantitative results in Fig. 16. We evaluated error for the ColorChecker Nano and, separately, our homemade chart of fabric swatches. The LLS and NNLS solves yielded similar color accuracy for both material sets, although unexpectedly NNLS slightly outperformed LLS. We suspect the image subtraction required for LLS contributed to increased error by compounding sensor noise. Thus, the slight theoretical improvement of LLS did not outweigh the simplicity of single-shot acquisition with NNLS. The chart panorama technique of Sec. 3.2 yielded slightly superior color accuracy compared with the faster capture method of Sec. 3.5. However, the error is still low for the fast method since its limited spectral angular resolution is mitigated by the fact that diffuse surfaces integrate illumination from a wide area of the environment.

For each image of Figs. 13 and 14, the fabric colors were reproduced nearly as accurately as the ColorChecker squares, showing that the chart-based solve generalized well to materials with other reflectance spectra. The yellow bowl in the still life even contained

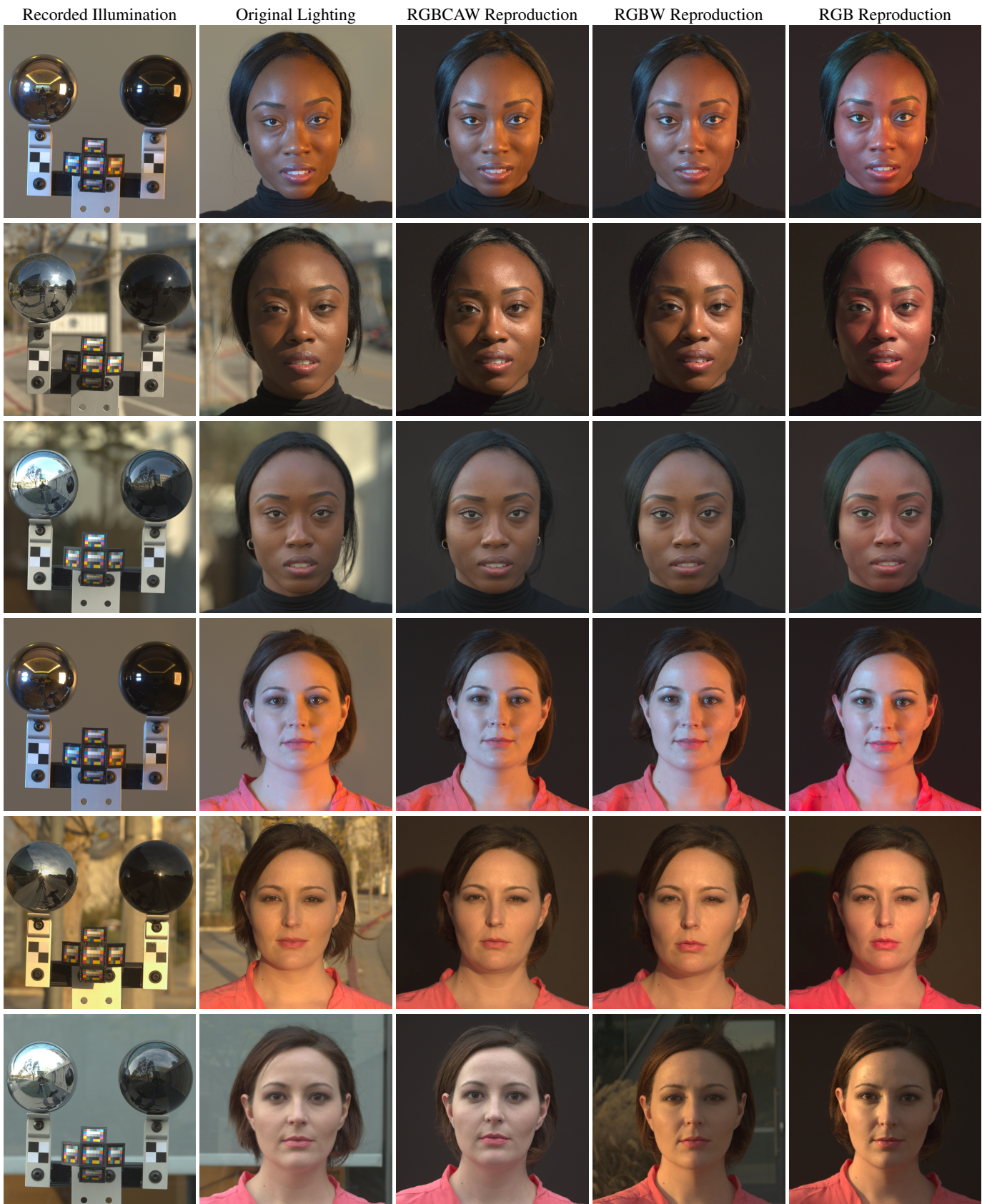


Figure 12: Two subjects in a variety of lighting environments (left columns) with three different lighting reproduction techniques. Generally, RGBCAW and RGBW reproduction produces accurate results, whereas using just RGB LEDs tends to oversaturate colors. The final two images of the bottom row show the subject and camera rotated 90 degrees to the left in the same sunset lighting of the fifth row, with RGBCAW lighting reproduction.

ACM Trans. Graph., Vol. 35, No. 4, Article 32, Publication Date: July 2016



Figure 13: Comparing the illumination capture techniques of Sections 3.5 and 3.2, using 6-channel RGBCAW illumination.

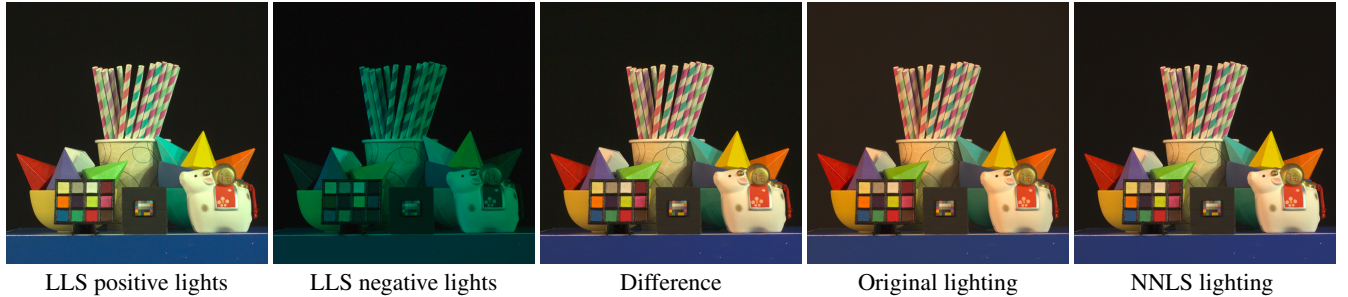


Figure 14: Comparing linear least squares (LLS) solves with positive and negative LED intensities (photographed in separate images) to nonnegative least squares (NNLS) solves, which can be photographed in a single image, using 6-channel RGBCAW illumination.

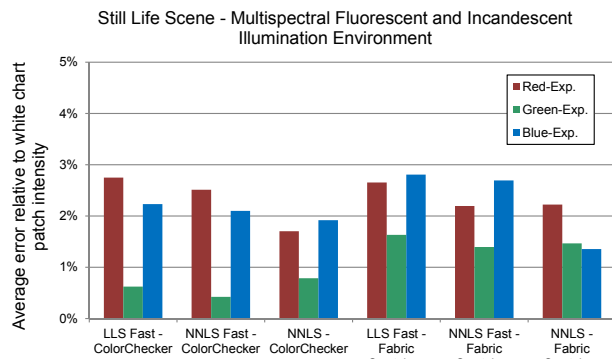


Figure 16: Quantitative experimental error plot for Fig. 15, for the LLS and NNLS solves (RGBCAW), based on the average squared errors of raw pixel values from all 30 ColorChecker Nano patches and, separately reported, our 12 fabric swatches. “Fast” refers to the spheres-and-charts lighting capture method of Sec. 3.5, while no designation refers to the chart panorama technique of Sec. 3.2.

a fluorescent pigment (appearing yellow under our blue LED), and its appearance under the reproduced illumination also matched that of the real environment.

Fig. 17 compares the results of using interpolated observations from all five color charts of the fast lighting capture device to using the colors from only the front-facing chart, for the indoor environment of Fig. 12. The 5-chart example produces slightly richer colors and can be seen to match the original effect of the lighting in the fourth row of Fig. 12, but the effect is subtle. The color charts in Fig. 17 visualize the error between the actual appearance of the left-facing and right-facing color charts in the lighting capture device compared to their appearance under the reproduced illumination, showing slightly better matches for the 5-chart result. In this case, observing only a front-facing color chart achieves acceptable multispectral lighting reproduction.

Fig. 1 shows each subject in real and reproduced outdoor illumination using RGBCAW lighting, where compositing is used to place the subject in the light stage on top of the original background. The alpha matte was obtained by taking a second silhouetted photograph a fraction of a second after the first, with the LED lights off, and the foamcore background lit brightly with a pair of flashes. The result are images where it is easy to believe that the subject is really in the environment instead of in the light stage, and the lighting reproduction is close to the original.

Fig. 18 shows our technique applied to an image sequence with dynamic lighting, where an actor is rolled through a set with fluorescent, incandescent, and LED lights with various colored gels applied. We reconstructed the full dynamic range of the illumination using the chrome and black sphere reflections and generated a dynamic RGBCAW lighting environment using the fast capture technique of Sec. 3.5. The lighting was played in the light stage as the actor repeated the performance in front of a green screen. Finally, the actor was composited into a clean plate of the set. The real and reproduced lighting scenarios are similar, although differences arise from discrepancies in the actor’s pose and some spill light from the green screen, especially under the hat, and some missing rim light blocked by the green screen. We ensured that the automated matting technique did not alter the colors of the foreground element, and better matte lines could be achieved by a professional compositor. (We have also implemented infrared matting with two cameras as in Debevec et al. [2002].) The limited lighting resolution of the LED sphere can be seen in the shadows of the hat on the face, though not much in the eye reflections. Overall, the lighting is effectively reproduced from the original set to the LED sphere.

5 Discussion

A strength of our technique is that it does not require measurement, knowledge, or estimation of any spectral illumination or reflectance functions; we just need to know how our camera sees a color chart lit by the desired section of the environment and lit by each of the

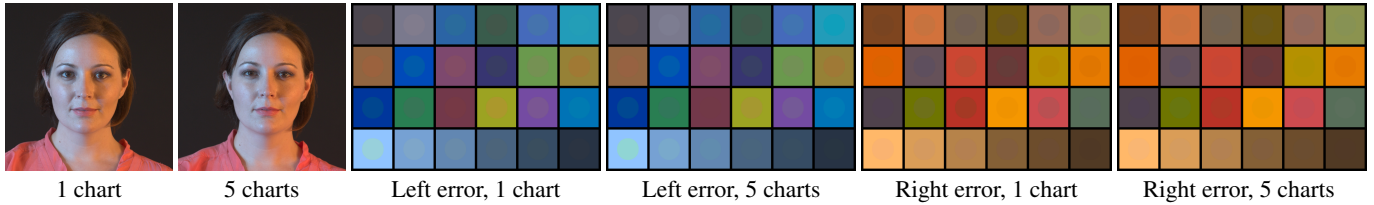


Figure 17: Comparison of single-chart reconstruction versus five-chart reconstruction.



Figure 18: Frames from an image sequence where a subject moves through an environment, causing dynamic lighting from fluorescent, incandescent, and LED lights with various gels and diffusers. The last column composites the subject onto a clean plate of the set.

differently colored LEDs. We could alternately have measured the spectra of the LED sources as well as the spectrum of every lighting direction in the environment, and then approximated the incident illumination spectra using linear combinations of the LEDs. Such a technique would require spectral measurement equipment and would likely be cumbersome for lighting capture.

Alternatively, to avoid omnidirectional spectral illumination capture, we could use the approach of Shi et al. [2014] to estimate illuminant spectra directly from color chart appearances once the HDRI maps were fused with color chart observations as in Sec. 3.4, and then approximate these spectra with linear combinations of LEDs. This approach still requires color chart spectral reflectance measurements and, also, has only been shown to accurately reconstruct smooth illuminant spectra. In contrast, we showed good color matching even for a spiky fluorescent source (Figs. 4, 5).

In either alternative approach with explicit spectral modeling, errors made in approximating the illuminant spectra with the LEDs will not necessarily be minimal with respect to how the camera will see materials lit by these spectra. Since we optimize directly so that the LEDs illuminate the color charts the way they appeared in the original lighting, there is theoretically no better lighting reproduction solution to be had from the observations available.

6 Future Work

We currently consider only the visible spectrum of light. Nonetheless, the ability to record and reproduce hyperspectral illumination with IR and UV components could have applications in medicine, garment design, and night vision research. Adding hyperspectral sensors and chart patches (and LEDs as in Ajdin et al. [2012]) could extend the technique into this domain.

Since the ColorChecker has only nineteen distinct spectra, it may fail to record information in certain areas of the spectrum where an item, such as a particular garment, has interesting spectral detail. In this case, a sample of the item could be added to the color chart, and the L matrices and lighting capture could proceed with this additional spectral detail taken into consideration. Furthermore, if a particular item's colors are not being reproduced faithfully, its weight in the nonnegative least squares solve could be increased, improving its color rendition at the expense of the other patches.

While our technique tailors the lighting reproduction to look correct to the camera, it does not specifically attempt to replicate the effects of the illumination as seen by the human eye. Empirically, for RGB-BCAW and RGBW lighting, the subject does appear similarly lit to their original lighting (though it is often dimmer than the original

environment), and RGB-only solves look even worse to the eye than to the camera for which the solution has been optimized. We could tailor the lighting reproduction to the human eye by measuring the L matrices for the color chart and LEDs in the photometric XYZ color space, by measuring each color chart square lit by each LED color with a spectroradiometer, building the L matrix from reported XYZ values. We could also optimize for multiple simultaneous observers, such as for both photographer and their camera.

7 Conclusion

In this paper, we have presented a practical way to reproduce complex, multispectral lighting environments inside a light stage with multispectral light sources. The process is easy to practice, since it simply adds a small number of color chart observations to traditional HDR lighting capture techniques, and the only calibration required is to observe a color chart under each of the available LED colors in the sphere. The technique produces visually close matches to how subjects would actually look in real lighting environments, even with as few as four available LED spectra (RGB and white), and can be applied to dynamic scenes. The technique may have useful applications in visual effects production, virtual reality, studio photography, cosmetics testing, and clothing design.

Acknowledgements

The authors wish to thank Randy Hill, Kathleen Haase, Christina Trejo, Greg Downing, Jamison Moore, Mark Bolas, Jessica Robertson, Jonetta Thomas, Donna Ruffin, Dan Sherlock, Joe di Gennaro, Keith Snail, Kathryn Rock, and the Natick Soldier Systems Center for their important support of this work. This project was sponsored by the U.S. Army Research Laboratory (ARL) under contract W911NF-14-D-0005 and in part by Qualcomm and a USC Annenberg Ph.D. Fellowship. The content of the information does not necessarily reflect the position or the policy of the Government, and no official endorsement should be inferred.

References

- AJDIN, B., FINCKH, M., FUCHS, C., HANIKA, J., AND LENSCHE. 2012. Compressive higher-order sparse and low-rank acquisition with a hyperspectral light stage. Tech. rep., Univ. of Tuebingen.
- DEBEVEC, P., WENGER, A., TCHOU, C., GARDNER, A., WAESE, J., AND HAWKINS, T. 2002. A lighting reproduction approach to live-action compositing. In *Proc. 29th Annual Conference on Computer Graphics and Interactive Techniques*, ACM, New York, NY, USA, SIGGRAPH '02, 547–556.
- DEBEVEC, P., GRAHAM, P., BUSCH, J., AND BOLAS, M. 2012. A single-shot light probe. In *ACM SIGGRAPH 2012 Talks*, ACM, New York, NY, USA, SIGGRAPH '12, 10:1–10:1.
- DEBEVEC, P. 1998. Rendering synthetic objects into real scenes: Bridging traditional and image-based graphics with global illumination and high dynamic range photography. In *Proc. of the 25th Annual Conf. on Computer Graphics and Interactive Techniques*, ACM, New York, NY, USA, SIGGRAPH '98, 189–198.
- GU, J., AND LIU, C. 2012. Discriminative illumination: Per-pixel classification of raw materials based on optimal projections of spectral brdf. In *Computer Vision and Pattern Recognition (CVPR), 2012 IEEE Conference on*, 797–804.
- HAMON, P.-L., HARMER, J., PENN, S., AND SCAPEL, N. 2014. Gravity: Motion control and face integration. In *ACM SIGGRAPH 2014 Talks*, ACM, New York, NY, USA, SIGGRAPH '14, 35:1–35:1.
- KANG, S. B., UYTENDAELE, M., WINDER, S., AND SZELISKI, R. 2003. High dynamic range video. *ACM Trans. Graph.* 22, 3 (July), 319–325.
- KAWAKAMI, R., ZHAO, H., TAN, R. T., AND IKEUCHI, K. 2013. Camera spectral sensitivity and white balance estimation from sky images. *Int. J. Comput. Vision* 105, 3 (Dec.), 187–204.
- KIDER, JR., J. T., KNOWLTON, D., NEWLIN, J., LI, Y. K., AND GREENBERG, D. P. 2014. A framework for the experimental comparison of solar and skydome illumination. *ACM Trans. Graph.* 33, 6 (Nov.), 180:1–180:12.
- KITAHARA, M., OKABE, T., FUCHS, C., AND LENSCHE, H. 2015. Simultaneous estimation of spectral reflectance and normal from a small number of images. In *Proceedings of the 10th International Conference on Computer Vision Theory and Applications*, VISAPP 2015, 303–313.
- MCCAMY, C., MARCUS, H., AND DAVIDSON, J. 1976. A color rendition chart. *Journal of Applied Photographic Engineering* 2, 3 (June), 95–99.
- PARK, J., LEE, M., GROSSBERG, M. D., AND NAYAR, S. K. 2007. Multispectral Imaging Using Multiplexed Illumination. In *IEEE International Conference on Computer Vision (ICCV)*.
- REINHARD, E., WARD, G., PATTANAIK, S., AND DEBEVEC, P. 2005. *High Dynamic Range Imaging: Acquisition, Display, and Image-Based Lighting*. Morgan Kaufmann Publishers Inc., San Francisco, CA, USA.
- RUMP, M., ZINKE, A., AND KLEIN, R. 2011. Practical spectral characterization of trichromatic cameras. *ACM Trans. Graph.* 30, 6 (Dec.), 170:1–170:10.
- SHI, J., YU, H., HUANG, X., CHEN, Z., AND TAI, Y. 2014. Illuminant spectrum estimation using a digital color camera and a color chart. In *Proc. SPIE*, 927307–927307–9.
- STUMPFEL, J., TCHOU, C., JONES, A., HAWKINS, T., WENGER, A., AND DEBEVEC, P. 2004. Direct hdr capture of the sun and sky. In *Proceedings of the 3rd Intl. Conf. on Computer Graphics, Virtual Reality, Visualisation and Interaction in Africa*, ACM, New York, NY, USA, AFRIGRAPH '04, 145–149.
- TOMINAGA, S., AND FUKUDA, T. 2007. Omnidirectional scene illuminant estimation using a multispectral imaging system. In *Proc. SPIE*, 649313–649313–8.
- TOMINAGA, S., AND TANAKA, N. 2001. Measurement of omnidirectional light distribution by a mirrored ball. In *The 9th Color Imaging Conference: Color Science and Engineering: Systems, Technologies, Applications, CIC 2001, Scottsdale, Arizona, USA, November 6-9, 2001*, 22–26.
- TOMINAGA, S., AND TANAKA, N. 2006. Omnidirectional scene illuminant estimation using a mirrored ball. *Journal of Imaging Science and Technology* 50, 3 (May), 217–227.
- UNGER, J., AND GUSTAVSON, S. 2007. High-dynamic-range video for photometric measurement of illumination. In *Proc. SPIE*, 65010E–65010E–10.
- WENGER, A., HAWKINS, T., AND DEBEVEC, P. 2003. Optimizing color matching in a lighting reproduction system for complex subject and illuminant spectra. In *Proceedings of the 14th Eurographics Workshop on Rendering*, Eurographics Association, Aire-la-Ville, Switzerland, EGRW '03, 249–259.